CHEMISTRY OF MATERIALS

pubs.acs.org/cm

Article

Deuteration-Enhanced Negative Thermal Expansion and Negative Area Compressibility in a Three-Dimensional Hydrogen Bonded Network

Piotr Rejnhardt,* Jan K. Zaręba, Andrzej Katrusiak, and Marek Daszkiewicz*

Cite This: *Chem. Mater.* 2023, 35, 5160−5167

Read Online

ACCESS | Metrics & More | Article Recommendations | Supporting Information

ABSTRACT: Negative area compressibility (NAC) and negative thermal expansion (NTE) are material behaviors raising high hope for applications such as ultrasensitive manometry and thermometry. However, the group of NAC materials is primarily limited to two-dimensional (2D) coordination compounds whose layered structure is prone to bidirectional compression when pressurized. Here, we report an alternative strategy that does not employ the formation of metal−organic systems but takes advantage of the pliability of hydrogen-bonded networks for searching materials with very rare NLC and NAC behaviors. Indeed, a strong NAC property, coupled with large NTE, has been identified for the hydrogen-bonded hydrochloride salt of L-arginine homologue (*S*)-2-amino-3-guanidinopropanoic acid monochloride − (HAmGP)Cl and its deuterated analogue − (DAmGP)Cl. While both structures feature isostructural phase transition at ca. 0.88 GPa, it is discovered that the replacement of protium with deuterium significantly boosts NAC magnitudes: phase II of (DAmGP)Cl features over two-fold higher negative area compressibility coefficient than that of the nondeuterated analogue ($\beta_{2,3}$ = −17.6(27) TPa^{-1} for (DAmGP)Cl vs −7.9(38) TPa^{-1} for HAmGP)Cl. Remarkably, the obtained value is the second largest area compressibility coefficient known for any material. What is more, deuteration enhances also the NTE property (α_2 = −23.4(22) vs −16.1(31) MK^{-1} for (DAmGP)Cl and (HAmGP)Cl, respectively) of the investigated supramolecular network. Our research opens new paths to the preparation of organic hydrogen-bonded materials with unique mechanical responsiveness to temperature and pressure stimuli.

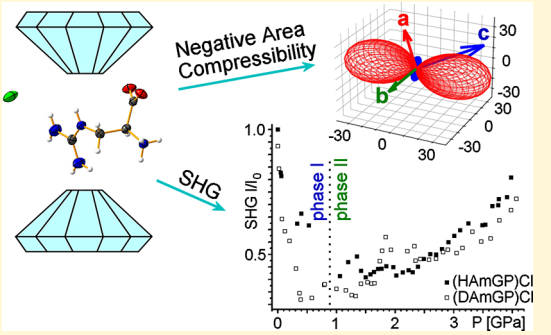

INTRODUCTION

Negative thermal expansion (NTE) and negative linear or area compressibility (NLC and NAC, respectively) are unusual responses to temperature and pressure changes that continuously attract the attention of the materials community.[1,2] The negative expansion is atypical material behavior in which crystals expand in one, two, or all three dimensions upon cooling, rather than compress in all directions as one normally expects due to, e.g., bond shortening and freezing of molecular motions. Negative compressibility (NC), in turn, touches upon a few materials whose crystal structures expand in one or two directions in response to the increasing hydrostatic pressure; these two different variants of negative compressibility are referred to as negative linear compressibility (NLC) and negative area compressibility (NAC), respectively.[3,4] Current struggle is to explore the fundamental features and mechanisms of those processes and to identify material classes that are the most prone to show unconventional responses to pressure and temperature. Unique mechanical responsiveness to thermal and pressure stimuli can be harnessed to generate functionalities that otherwise would be challenging to obtain. For example, the NTE materials can be potentially used in controlled thermal expansion composites such as fiber optics coatings or mirror substrates, while materials displaying the NC phenomenon are seen as smart materials that can "counteract" the pressure impact, e.g., materials increasing the sensitivity of pressure sensors[5] or as artificial muscles in state-of-the-art body armors.[6−8]

There are signposts to indicate which crystalline materials are likely to show anomalous mechanical phenomena. Experimental data show that NTE materials typically display also the NLC phenomenon,[9−11] that is, the temperature-induced shortening and pressure-induced expansion take place along the same crystallographic direction, but the actual nature of structural deformation does not necessarily has to be the same.[12] NLC occurrence was identified for selected molecular compounds,[13,14] inorganic materials,[15,16] and coordination polymers,[3,17] including metal−organic frameworks (MOFs).[9,10] The latter class of compounds constitutes the

Received: April 12, 2023
Revised: June 2, 2023
Published: June 23, 2023

attractive groundwork for studies of NLC and related phenomena, as the strength of coordination bonds and porous structure facilitate large structural deformations along with raising pressure. Especially materials with wine-rack motifs in their structure, which usually expand along the longer diagonal and shrink along the shorter diagonal under compression, have a high probability of having NLC property.[18]

In the case of NAC, which is an even more exotic phenomenon, the bidirectional structural expansion upon pressure stress usually stems from the flattening of the structured 2D coordination layers, typically of quadrangular rings or honeycomb-like topology. This mechanism exists in MOF structures, e.g., $Zn(CH_3COO)_2{\cdot}2H_2O$,[4] $[Zn(L)_2(OH)_2]_n{\cdot}H_2O$, where L is 4-(1H-naphtho[2,3-*d*]-imidazole-1-yl)benzoate,[19] or in inorganic 2D structures such as KBBF[20] and $TlGaSe_2$.[21] It is thus clear that searching for novel materials with NLC or NAC properties leads to design and synthesis of 2D coordination compounds with targeted topologies. On the other hand, quite interesting is the scarcity of reports on NAC materials where the mechanism of structural expansion is only based on distance changes between donor and acceptor atoms of hydrogen-bonded systems. This raises the question of whether there are any fundamental limitations which preclude purely supramolecular networks from showing this property, or whether the elastic behavior of 3D-hydrogen bonded systems is just an uncharted territory of high-pressure crystallography that calls for exploration.

We propose to exploit the inherent plasticity of hydrogen bonds, which have the capability to dramatically change their geometry, potentially to a greater extent than could be achieved by more rigid coordination bonds. By pursuing this idea, we have obtained and investigated with the use of temperature and high-pressure crystallography, as well as second harmonic generation (SHG) measurements, salt of L-arginine homologue (*S*)-2-amino-3-guanidinopropanoic acid monochloride - (HAmGP)Cl. This 3D-hydrogen bonded compound, crystallizing in space group $P2_1$, features the NTE property in its ambient-pressure phase I, but more importantly, also undergoes a high-pressure isostructural phase transition to phase II which displays strong NAC characteristics. On top of that, it was also discovered that the strength of NLC and NAC effects can be boosted by the isotopic exchange of all labile protons for deuterium atoms. In the case of NAC, deuteration leads to over two-fold enhancement of the negative area compressibility coefficient.

EXPERIMENTAL SECTION

Synthesis of (HAmGP)Cl. The starting compounds, (*S*)-2-amino-3-guanidinopropanoic acid dichloride $(H_2AmGP)Cl_2$ (ArkPharm Inc., 90% purity) and ammonia solution ($NH_3{\cdot}H_2O$) (POCh, 25%), were used as supplied. $(H_2AmGP)Cl_2$ (0.5 mmol, 0.110 g) was dissolved in 4 mL (1 mmol) of ammonia solution. Colorless, prism-shaped crystals of (*S*)-2-amino-3-guanidinopropanoic acid monochloride were obtained after 1 day by slow evaporation of the mixture. The starting compounds, (*S*)-2-amino-3-guanidinopropanoic acid dichloride $(H_2AmGP)Cl_2$ (ArkPharm Inc., 90% purity) and ammonia solution ($NH_3{\cdot}H_2O$) (POCh, 25%), were used as supplied. $(H_2AmGP)Cl_2$ (0.5 mmol, 0.110 g) was dissolved in 4 mL (1 mmol) of ammonia solution. Colorless, prism-shaped crystals of (*S*)-2-amino-3-guanidinopropanoic acid monochloride were obtained after 1 day by slow evaporation of the mixture.

Synthesis of (DAmGP)Cl. Deuterium oxide (D_2O) (Aldrich, 99%) was used as supplied. The (HamGP)Cl (0.0719 g) was dissolved in 1 mL of deuterium oxide. Colorless crystals of (DamGP)Cl were obtained after ca. 3 days by slow evaporation of the mixture. The procedure was carried out three times. Finally, well-shaped deuterated crystals were obtained after 10 days. The degree of deuteration was estimated to be about 60% based on nuclear magnetic resonance (NMR) spectra measured in DMSO-d_6.

Temperature and Pressure Single-Crystal X-ray Diffraction. X-ray diffraction data were collected on an Oxford Diffraction four-circle single-crystal Xcalibur diffractometer equipped with a CCD detector using graphite-monochromated MoKα radiation (λ = 0.71073 Å). The raw data were processed with the CrysAlis data reduction program (version 1.171.38.43). The intensities of the reflections were corrected for Lorentz and polarization effects. The crystal structures were solved by direct methods[23] and refined by the full-matrix least-squares method using SHELXS incorporated in OLEX2.[24,25] RIGU and ISOR restraints were used for stabilizing the refinement of the structure model in high pressure. Nonhydrogen atoms were refined using anisotropic displacement parameters. All H-atoms were visible on the Fourier difference maps, but placed by geometry and allowed to refine by riding on the parent atom. Visualizations of the structure were made using Diamond3.2k[26] and Mercury programs.[27] High-pressure X-ray diffraction experiments were carried out using a Merrill−Bassett diamond anvil cell (DAC), where single crystals of (HAmGP)Cl and (DAmGP)Cl were placed inside. Polydimethylsiloxane oil (Wacker Chemie) was used as a pressure medium. The hydrostatic conditions for this pressure medium were checked, and they were preserved at least up to 4 GPa. Pressure was calibrated using an Ocean Optics USB 4000 spectrometer by the ruby-fluorescence method[28] with a precision of 0.05 GPa and taking into account the temperature correction.[29] High-pressure diffraction data were collected at 19 pressure points for (HAmGP)Cl and 12 pressure points for (DAmGP)Cl. Low-temperature X-ray diffraction experiments were carried out using an OxfordCryosystems device in the range of 400−84 K. Low-temperature diffraction data were collected at 23 temperature points for (HAmGP)Cl and 15 temperature points for (DAmGP)Cl.

Spectroscopic Measurements. Room-temperature FT−IR spectra were measured on a Bruker IFS-88 spectrometer in the range of 4000−400 cm^{-1} with 2 cm^{-1} resolution. Nujol and fluorolube mull techniques have been used in the measurements. A closed-cycle helium cryostat system from APD Cryogenics Inc. (DE-202 expander, compressor model HC-2, microprocessor-based temperature indicator/controller model 5500-1-25) was used for low-temperature measurements (300−12 K). The temperature of the sample was maintained with an accuracy of ±0.1 K. ^{1}H NMR spectra were measured in DMSO-d_6 on a Bruker Avance 500 spectrometer operating at 500 MHz (^{1}H).

SHG Measurement. Measurements of the relative intensity of the second harmonic generation (Kurtz−Perry)[30] were performed for powder samples and for potassium dihydrogen phosphate (KDP) which was the reference compound. Prior to measurement, monocrystals of measured compounds and KDP were crushed using a spatula and then sieved with an Aldrich mini-sieve set, collecting crystal fractions of 177−125 μm. The obtained powders with a known particle size were tightly packed between microscope slides, forming a homogeneous layer. The salt and KDP samples were excited in exactly the same geometry with 800 nm femtosecond laser pulses, 1 kHz repetition rate, and 130 fs pulse length, generated by a Quantronix Integra-C regenerative amplifier. Scattered excitation radiation was filtered using a short-pass filter (Thorlabs FESH0700). SHG spectra were collected with an Ocean Optics Flame T spectrometer.

The source of the femtosecond pulses for the measurements of the SHG as a function of pressure was the Coherent Astrella Ti: sapphire regenerative amplifier. This amplifier generates laser pulses with a wavelength of 800 nm, a repetition rate of 1 kHz, and a pulse length of 75 fs. To generate high pressure, the Merrill−Bassett DAC was used, as well as a tripod made especially for these measurements, which ensured a precise and repeatable arrangement of the DAC on the optical table in relation to the excitation source and measurement optics. The SHG spectra as a function of pressure were collected with an Ocean Optics Flame T spectrometer. Scattered excitation radiation

https://doi.org/10.1021/acs.chemmater.3c00870
Chem. Mater. 2023, 35, 5160−5167

was filtered using a short-pass filter (Thorlabs FESH0700). To calibrate the pressure inside the DAC, the ruby fluorescence method[28] was used, using an Avantes AvaSpec EVO4096 high-resolution spectrometer (slit width of 5 μm) and taking into account the temperature correction.[29] Ruby fluorescence was excited by a laser pointer generating continuous radiation of 532 nm with a power of about 20 mW. Scattered excitation radiation was filtered using a long-pass filter (Thorlabs FELH650). Pressure was calibrated with a precision of 0.05 GPa. *Caution! Work with the high-power laser brings danger to the eyes, especially in spectral range in which the beam is invisible. Adequate eye protection should be used during measurements.*

RESULTS AND DISCUSSION

The title compound (HAmGP)Cl and its deuterated analogue (DAmGP)Cl both crystallize in noncentrosymmetric, space group $P2_1$. Comparison of molecular structures of both compounds to the other known salts of (*S*)-2-amino-3-guanidinopropanoic acid reveals a significant difference in the arrangement of the terminal groups (Figure 1).[31] The

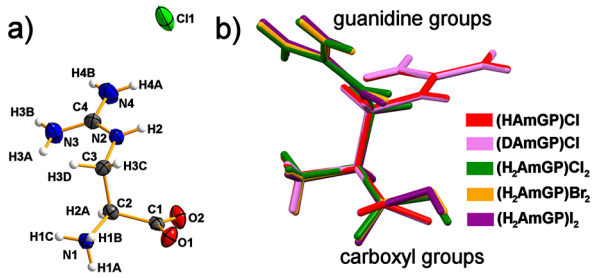

Figure 1. (a) Molecular structure of (*S*)-2-amino-3-guanidinopropanoic acid monochloride; (b) shows differences of conformation for a series of organic salts with (*S*)-2-amino-3-guanidinopropanoic acid cation.

guanidinium and carboxyl groups lie much closer to each other in (HAmGP)Cl than in dihalogen salts. A series of single-crystal X-ray diffraction (SC-XRD) experiments in the temperature range of 400−84 K revealed that there are no temperature-induced structural phase transitions. However, SC-XRD experiments showed an abnormal decrease of the lattice parameter *c* upon heating for both studied structures (Figure 2a). These data were used to calculate expansion coefficients and the indicatrix (Figure 3a,c, Table S1). The blue part refers to the NTE behavior: $\alpha_1 = -16.1(31)$ MK^{-1} for (HAmGP)Cl and $\alpha_2 = -23.4(22)$ MK^{-1} for deuterated analogue (DAmGP)Cl. Compared to the other NTE materials, the results are quite impressive as for organic 3D structures. For example, the negative thermal coefficient of (DAmGP)Cl is surprisingly on a par with those for MOF materials such as $CdSO_4$-type [Ag(mim)] (−24.5(8) MK^{-1})[11] and HMOF-1 (−21(3)MK^{-1}).[32] Compression of the crystal revealed first-order high-pressure isostructural phase transition, within the same space group $P2_1$, at 0.88 and 0.86 GPa for (HAmGP)Cl and (DAmGP)Cl, respectively (Figures 2b and 4). The reversible nature of phase transition was confirmed by the decompression of the crystals which led to the restoration of initial unit-cell parameters. An unusual feature of the phase transition is a change of monoclinic β angle which leaps from obtuse to acute angle in phase II (Figures S1 and S2). Although it means that the angle is temporarily the right angle, the higher orthorhombic symmetry was not observed due to the discontinuous nature of the phase transition. Impact of the pressure-induced phase transition on the crystal shape was

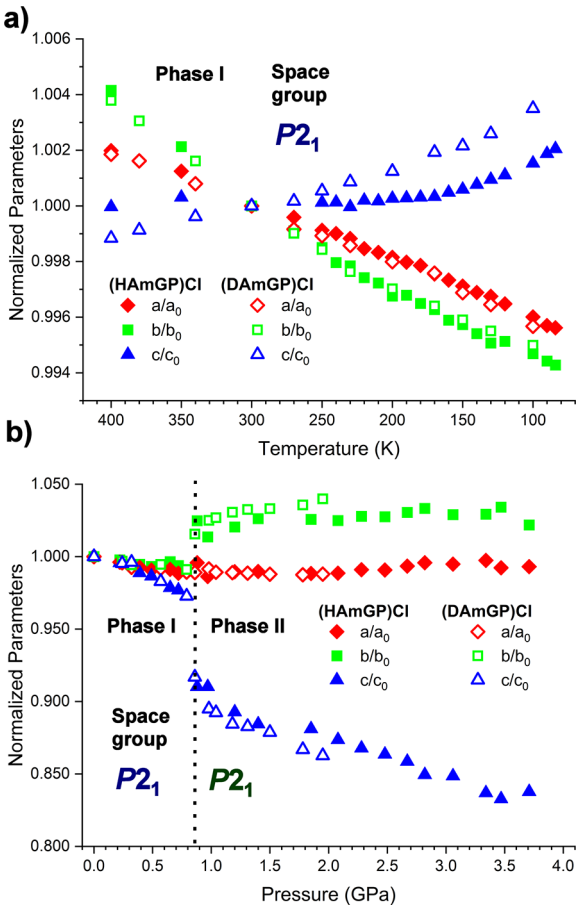

Figure 2. Relative thermal expansion (a) and compression (b) of lattice parameters *a*, *b*, and *c* for (HAmGP)Cl (full symbols) and (DAmGP)Cl (open symbols).

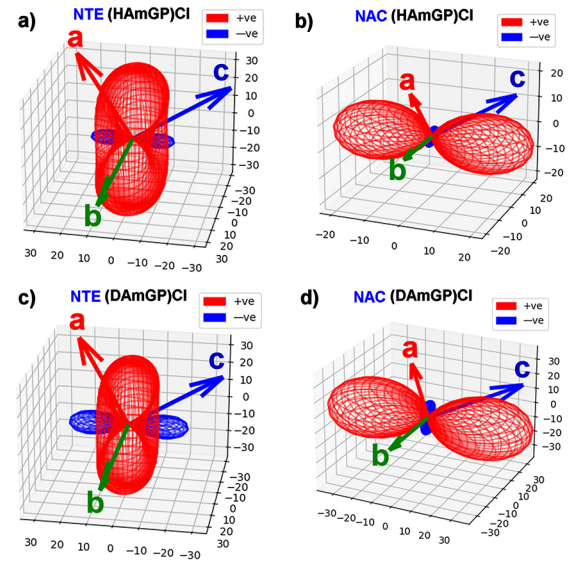

Figure 3. Indicatrices of (a) thermal expansion for phase I and (b) compressibility for phase II of (HAmGP)Cl, (c) thermal expansion for phase I and (d) compressibility for phase II of (DAmGP)Cl (*a*, *b*, and *c* axes are crystallographic directions).[22]

observed with an optical microscope. Three crystals of the known orientations of the lattice vectors were mounted into the chamber of DAC, where the main crystallographic

https://doi.org/10.1021/acs.chemmater.3c00870
Chem. Mater. 2023, 35, 5160−5167

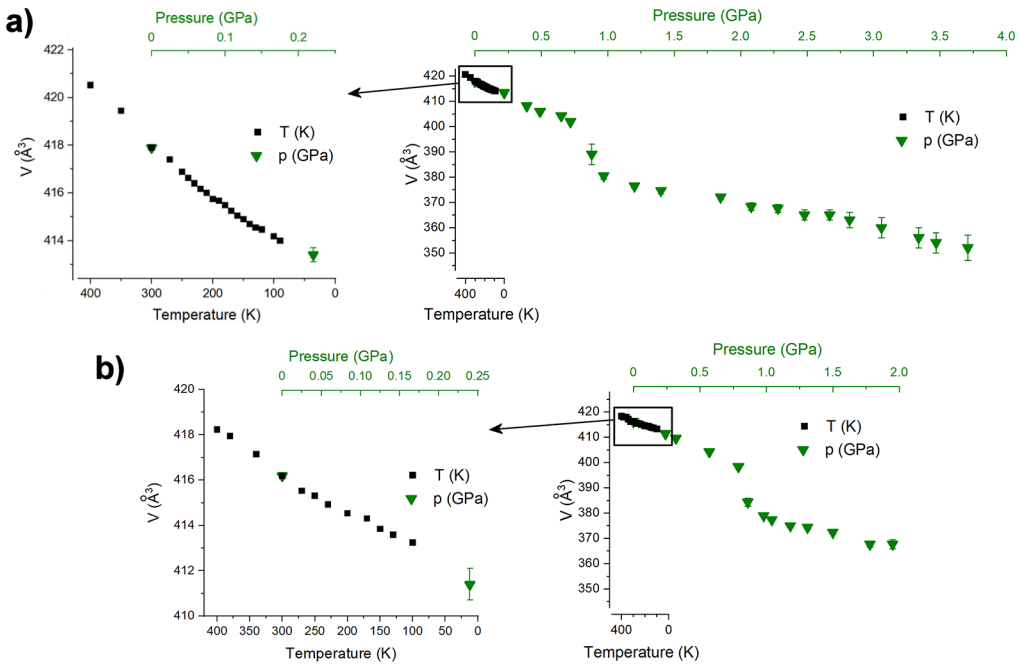

Figure 4. Changes of the unit cell volume as a function of temperature and pressure for (a) (HAmGP)Cl and (b) (DAmGP)Cl. The pressure scale was adjusted to the temperature scale by adapting the volume change trends for both thermodynamic parameters.

directions were perpendicular to the diamond's cullet. After the phase transition, it was possible to observe small changes in the shape of two crystals oriented along *a* and *b* axes (Figure 5). This kind of multicrystal approach in high-pressure experiments using DAC has been done before for example to increase the completeness of collected X-ray diffraction data.[33]

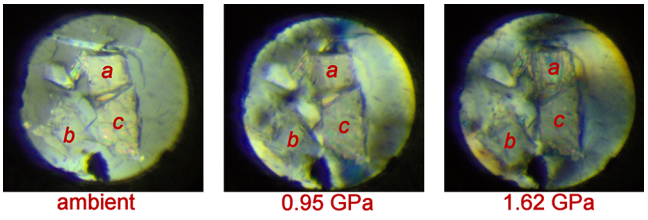

Figure 5. Three oriented crystals mounted inside the Merrill–Bassett diamond anvil cell (DAC). Lattice parameters *a*, *b*, and *c* are perpendicular to the crystal faces seen in the photographs.

The juxtaposed values of the unit-cell volume from temperature and pressure SC-XRD experiments (Figure 4) show that the unit-cell volume at 100 K corresponds to that measured at 0.17 GPa. The further squeezing of the crystal causes a reduction of the unit cell volume, which is far beyond the reach of liquid-nitrogen cooling at atmospheric pressure. A series of IR spectra confirmed the stability of phase I down to 12 K (Figure S3). This fact can be explained on the basis of the *V* vs *p*/*T* plots. The pressure-induced transition to phase II takes place when the unit cell volume decreases below 400 Å^3, but the thermal-contraction interpolation of the volume down to 0 K is still larger by approximately 12 Å^3. Thus, only the application of the pressure as an external stimulus allows one to access the new phases for (HAmGP)Cl and (DAmGP)Cl.

The latest compilation of compression and thermal expansion correlation of the crystal volume showed that on average the effect of 0.2 to 0.5 GPa is similar to the changes caused by temperature between 300 and 100 K.[34] Both studied compounds (HAmGP)Cl and (DAmGP)Cl lie outside this range and do not behave like most organic or MOF crystals. The (HAmGP)Cl and (DAmGP)Cl crystals are softer, as the changes induced by colling down to 100 K correspond to a pressure of ca. 0.17 GPa.

The crystal structure of (HAmGP)Cl phases I and II can be described as a salt of organic and chloride ions. In ionic crystals, the cohesion forces are dominated by the electrostatic attraction and in (HAmGP)Cl additionally, a complex three-dimensional network of hydrogen bonds is formed. There are four NH···Cl$^-$, one NH$^+$···Cl$^-$, and three NH$^+$···O$^-$ independent hydrogen bonds. The hydrogen bonds NH$^+$···O$^-$ connect the HAmGP$^+$ cations into corrugated sheets extending in a plane (001), and these sheets are interconnected through the H-bonds to the Cl$^-$ anions, as shown in the autostereograms in Figure S4. The seven H-bonds in (HAmGP)Cl differ in their strength and directions in the crystal structure. For example, of the five H···Cl$^-$ bonds involving one Cl$^-$ anion, two bind it to one HAmGP$^+$ cation, two other H-bonds are binding it to another HAmGP$^+$ cation and the fifth H-bond is to yet another HAmGP$^+$ cation. Due to this relatively large number of directional interactions, there are considerable voids (Figure 6), mainly located around the five-fold H···Cl$^-$ bonded chlorine anions linking the corrugated NH$^+$···O$^-$ bonded sheets. The sheets are quite compact, and no such voids are present between the cations (Figure 6).

The mechanism of the NTE of phase I can be connected to its layered structure. The sheets are interconnected through the directional NH···Cl$^-$ bonds, five per one anion, which like columns are surrounded by void space (Figure 6). These directional interactions are gradually destabilized by increasing temperature. Consequently, the increasing temperature decreases the distance between the sheets parallel to the crystal planes (001) and reduces the length of the unit-cell parameter c (Figure 2a). The increased temperature expands the corrugated sheets, reduces their width, and in this way additionally contributes to the NTE. The ND···Cl are weaker[35]

https://doi.org/10.1021/acs.chemmater.3c00870
Chem. Mater. 2023, 35, 5160−5167

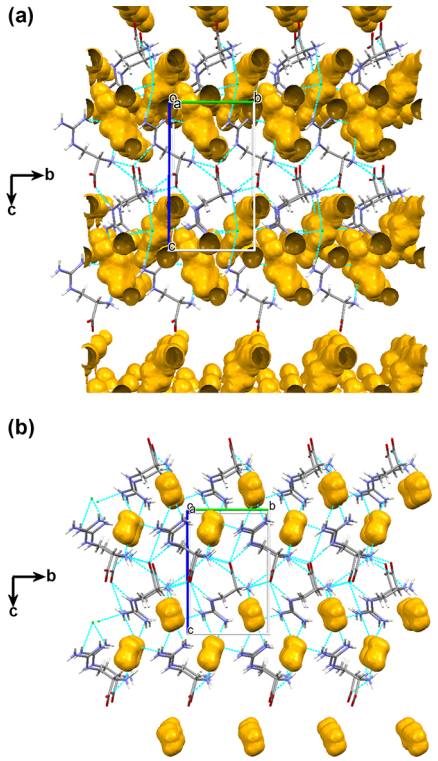

Figure 6. Autostereographic projections of the crystal structures and voids in (DAmGP)Cl: (a) phase I at 0.1 MPa and 295 K; and (b) phase II at 1.04 GPa and 295 K, viewed along the *a* direction (cf. Figure S4). The same probing sphere radius of 0.7 Å and step 0.1 Å applied for the calculations in program Mercury yielded the voids-to-volume ratio of (a) 13.2% and (b) 3.2%, respectively.

and are easier destabilized by thermal vibration. Hence, there is isotope enhancement of the NTE in the (HAmGP)Cl crystal.

The mechanism of phase transition also involves changes in molecular conformation. Torsion angles related to the geometry of the amino acid carbon chain, guanidinium and carboxyl groups decrease after phase transition (Figure S5). Accordingly, the side groups get closer to each other and the organic cation takes a more compact volume. As a result, a shrink of the unit cell crystal along the crystallographic *c* axis is clearly observed (Figures 7 and S2). It is reflected as a red part

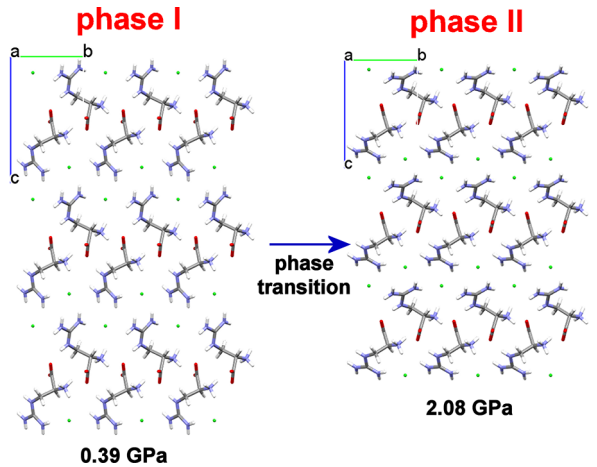

Figure 7. Corresponding portions of the (HAmGP)Cl crystal structure in phases I and II, viewed along the *a* axis.

of the compressibility indicatrix of a dumbbell shape (Figure 3b,d). Apart from this, elevated pressure affects the network of intermolecular interactions. In the 3D network of hydrogen bonds, the atypical change of weak N4−H4A···Cl1 interaction is worth noting. Here, the donor···acceptor distance increases during the phase transition above the van der Waals limit (Figure 8). This behavior is continued at higher pressures and is connected to negative area compressibility (NAC) for phase II of the studied crystals.

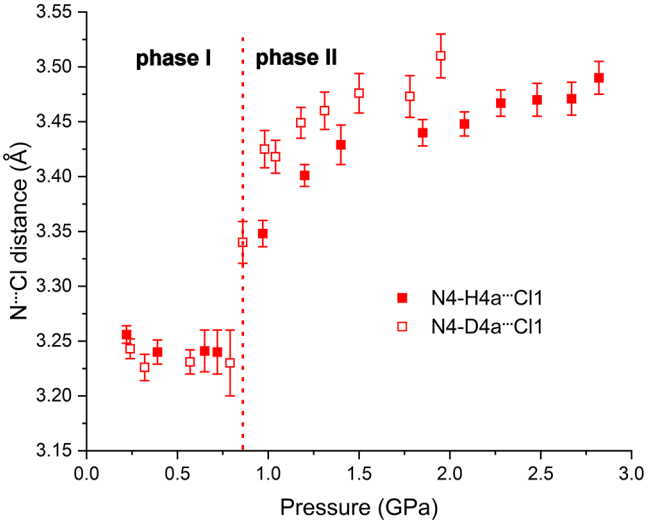

Figure 8. Pressure dependence of distance N···Cl for hydrogen bonds N4−H4a···Cl1 and N4−D4a···Cl1 in (HAmGP)Cl and (DAmGP)Cl.

A series of high-pressure experiments revealed an increase of two unit-cell parameters *a* and *b* for phase II. The data were used to calculate compressibility coefficients by PASCal software[22] (Table S2). Two negative values for (HAmGP)Cl, $\beta_2 = -4.5(24)$ TPa^{-1} and $\beta_3 = -3.4(14)$ TPa^{-1} reveal the NAC feature of this material which is seen as a blue toroidal part of the compressibility indicatrix (Figure 3b,d). The plane of the toroid is nearly parallel to the (−104) crystallographic plane and the magnitude of two-dimensional compressibility can be calculated as $\beta_{2,3} = \beta_2 + \beta_3 = -7.9(38)$. It turns out that compressibility coefficients are significantly higher for (DAmGP)Cl, with $\beta_2 = -10.8(10)$ TPa^{-1} and $\beta_3 = -6.8(17)$ TPa^{-1}, resulting in more than two times larger area compressibility coefficient, $\beta_{2,3} = \beta_2 + \beta_3 = -17.6(27)$ TPa^{-1} than that for the nondeuterated analogue.

Remarkably, the obtained value is the second largest area compressibility coefficient known for any material. While the "world record" for MOF of formula $[Zn(L)_2(OH)_2]_n$·guest ($\beta_{(001)} = -72(6)$ TPa^{-1}) is still unbeatable up-to-date,[19] it must be stressed that supramolecular hydrogen-bonded network (DAmGP)Cl features a more than twice higher β value than compounds of formulas Ag(tcm) ($\beta_{(010)} = -7.5(8)$ TPa^{-1})[36] and $Zn(CH_3COO)_2{\cdot}2H_2O$ ($\beta = -8.1(8)$ TPa^{-1}).[4,37]

At the phase transition at 0.9 GPa, the structure becomes more densely packed, at the cost of stability of $H^+\cdots Cl^-$ bonds and all directional interactions in general. Consequently, the hydrogen bonds $H^+\cdots Cl^-$ become weaker, longer (Figure 8), and usually more bent. On the transition to phase II, the void spaces are collapsed and the columns of weakened Cl-mediated hydrogen bonds are pushed into the grooves of the corrugated sheets, and they increased components of the vectors along

https://doi.org/10.1021/acs.chemmater.3c00870
Chem. Mater. 2023, 35, 5160−5167

$H^+\cdots Cl^-$ bonds pushing apart the folds of the corrugated sheets. It causes a strong NLC of the sheets along the *b* direction. The unit-cell parameter *a* is initially compressed in phase II, but starting from about 1.7 GPa it becomes longer with increased pressure, so the crystal acquires a very rare property of NAC, up to 3.2 GPa at least, according to our measurements. The strong isotope effect of deuteration on the crystal compressibility can be explained by the secondary geometric H/D isotope effect (Ubbelohde effect), which previously has been found to substantially modify the energetic landscape and geometry of hydrogen bonds[38−40] and their directional features weaker, too.[41,42] Hence, apart from the stronger elongation of the deuteron, $D^+\cdots Cl^-$ bonds in phase II, their weaker directionality results in more prevailing denser packing and stronger penetration into the grooves of corrugated sheets.[11]

Since both studied salts of (*S*)-2-amino-3-guanidinopropanoic acid crystallize without the inversion center and undergo the phase transition, second-order nonlinear optical properties were probed as a function of pressure. The relative efficiency of SHG response at room temperature and pressure for (HAmGP)Cl and (DAmGP)Cl is essentially the same, with 2.40 I_{KDP} and 2.24 I_{KDP}, respectively. The values are much greater than that for the related compound, L-arginine chloride monohydrate, 0.38 I_{KDP},[43] which is likely connected with the shorter carbon chain in both homologues. The π-electron clouds from guanidinium and carboxy groups are placed closer to each other in the studied compounds than in L-arginine. This fact may tune the polarizability among the homologues. What is more, the intensity of the SHG signal is significantly greater in comparison to the dichloride salt $(H_2AmGP)Cl_2$, 0.029 I_{KDP}.[31] It is reasonable to connect such a substantial difference to various conformation of cations (Figure 1b), especially lower separation of guanidinium and carboxy groups. Also, the deprotonated carboxy group in (HAmGP)Cl possesses a delocalized electron cloud over the whole group, which tunes the molecular polarizability. Elevated pressure significantly changes the intensity of the SHG signal (Figure 9). Both structures (HAmGP)Cl and (DAmGP)Cl are characterized by a decrease of SHG response up to high-pressure induced phase transition. Further squeezing the sample causes gradual increase in the SHG signal for phase II (Figure 9). It is reasonable to suppose that attenuation of the SHG signal of phase I is connected with positive compression which suppresses the polarizability of the molecule. The opposite effect is observed for phase II featuring the NAC phenomenon.

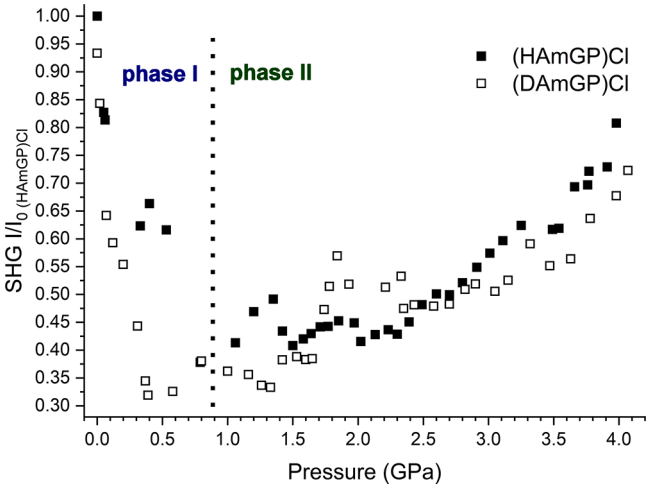

Figure 9. Intensity of SHG response as a function of pressure for (HAmGP)Cl and (DAmGP)Cl.

CONCLUSIONS

The title compound and its deuterated analogue undergo a pressure-induced isostructural phase transition at 0.88 and 0.86 GPa, respectively. At atmospheric pressure, phase II could not be obtained; the presence of phase I of (HAmGP)Cl is evidenced from as low as 12 K at least up to 400 K. We revealed the negative area compressibility for the crystal phase II. This extremely rare property was earlier reported only for a handful of compounds, including perovskite $PbTiO_3$,[44] NH-N bonded 2-methyl-benzymidazole,[45] but mainly the layered inorganic structures and coordination polymers. So far, to the best of our knowledge, NAC was not observed for such complex 3D hydrogen bonded network as that in (HAmGP)Cl and (DAmGP)Cl. Thus, the results for (HAmGP)Cl and (DAmGP)Cl challenge the extant belief that the structure composed of interactions/bonds of extremely different nature are key to the NAC. Furthermore, we show that NAC can be further tuned by deuteration since the phase II of the deuterated analogue has over two-fold higher negative compressibility coefficient than (HAmGP)Cl. Relative intensities of SHG response are impressive for both structures, (HAmGP)Cl and (DAmGP)Cl, at ambient conditions. Dramatic loss of the SHG response for phase I and its gradual restoration for phase II are observed. It appears that the three-dimensional shrinking of the crystal has a negative effect on the recorded signal (phase I). Since the negative area compressibility is observed for the phase II, we suppose that molecular separation in two dimensions increases polarizability, which enhances the nonlinear response. All in all, the reported compounds of (*S*)-2-amino-3-gunidinopropanoic acid can be used as a very sensitive pressure indicator because of high values of NAC coefficients.

ASSOCIATED CONTENT

Data Availability Statement

This material is available free of charge via the Internet at http://pubs.acs.org. CCDC 2160003−2160037 contain the supplementary crystallographic data for this paper. The data can be obtained free of charge from The Cambridge Crystallographic Data Centre via www.ccdc.cam.ac.uk/structures.

Supporting Information

The Supporting Information is available free of charge at https://pubs.acs.org/doi/10.1021/acs.chemmater.3c00870.

> β lattice parameter vs p/T plot; crystal packing viewed along *b* axis before and after phase transition; IR spectra; Autostereographic of the crystal structures of (HAmGP)Cl phases I and II; plots of torsional angles; a part of indicatrices of NTE and NAC; tables of thermal expansion coefficients and compressibility coefficients; crystal data and structure refinement details and geometry of hydrogen bonds; lattice parameters at various pressure conditions (PDF)

https://doi.org/10.1021/acs.chemmater.3c00870
Chem. Mater. 2023, 35, 5160−5167

AUTHOR INFORMATION

Corresponding Authors

Piotr Rejnhardt − *Institute of Low Temperature and Structure Research, Polish Academy of Sciences, 50-422 Wrocław, Poland; Faculty of Chemistry, University of Warsaw, 02-093 Warszawa, Poland*; Email: p.rejnhardt@chem.uw.edu.pl

Marek Daszkiewicz − *Institute of Low Temperature and Structure Research, Polish Academy of Sciences, 50-422 Wrocław, Poland*; orcid.org/0000-0002-1619-6146; Email: m.daszkiewicz@intbs.pl

Authors

Jan K. Zaręba − *Institute of Advanced Materials, Faculty of Chemistry, Wroclaw University of Science and Technology, 50-370 Wrocław, Poland*; orcid.org/0000-0001-6117-6876

Andrzej Katrusiak − *Faculty of Chemistry, Adam Mickiewicz University, 61-614 Poznań, Poland*; orcid.org/0000-0002-1439-7278

Complete contact information is available at: https://pubs.acs.org/10.1021/acs.chemmater.3c00870

Author Contributions

The manuscript was written through contributions of all authors. All authors have given approval to the final version of the manuscript.

Notes

The authors declare no competing financial interest.

ACKNOWLEDGMENTS

We would like to thank Prof. Jan Baran, ILT&SR PAS, for the measurements of the IR spectra. Prof. Elżbieta Wojaczyńska, Wroclaw University of Science and Technology, is gratefully acknowledged for the measurement and analysis of NMR spectra. P.R. and M.D. would like to thank ILT&SR PAS for financial support by statutory activity subsidy, no. 2019/S. J.K.Z. acknowledges support from Academia Iuvenum, Wroclaw University of Science and Technology.

ABBREVIATIONS

NTE, negative thermal expansion; NLC, negative linear compressibility; NAC, negative area compressibility; SHG, second harmonic generation; SC-XRD, single-crystal X-ray diffraction; DAC, diamond anvil cell

REFERENCES

(1) Sleight, A. W. Negative Thermal Expansion Materials. *Curr. Opin. Solid State Mater. Sci.* **1998**, *3*, 128−131.

(2) Lind, C. Two Decades of Negative Thermal Expansion Research: Where Do We Stand? *Materials* **2012**, *5*, 1125−1154.

(3) Cairns, A. B.; Goodwin, A. L. Negative Linear Compressibility. *Phys. Chem. Chem. Phys.* **2015**, *17*, 20449−20465.

(4) Feng, G.; Zhang, W. X.; Dong, L.; Li, W.; Cai, W.; Wei, W.; Ji, L.; Lin, Z.; Lu, P. Negative Area Compressibility of a Hydrogen-Bonded Two-Dimensional Material. *Chem. Sci.* **2019**, *10*, 1309−1315.

(5) Baughman, R. H.; Stafström, S.; Cui, C.; Dantas, S. O. Materials with Negative Compressibilities in One or More Dimensions. *Science* **1998**, *279*, 1522−1524.

(6) Polymer Sensors and Actuators. *Polymer Sensors and Actuators* 2000, DOI: 10.1007/978-3-662-04068-3.

(7) Aliev, A. E.; Oh, J.; Kozlov, M. E.; Kuznetsov, A. A.; Fang, S.; Fonseca, A. F.; Ovalle, R.; Lima, M. D.; Haque, M. H.; Gartstein, Y. N.; Zhang, M.; Zakhidov, A. A.; Baughman, R. H. Giant-Stroke, Superelastic Carbon Nanotube Aerogel Muscles. *Science* **2009**, *323*, 1575−1578.

(8) Baughman, R. H. Auxetic Materials: Avoiding the Shrink. *Nature* **2003**, *425*, 667.

(9) Zeng, Q.; Wang, K.; Zou, B. Large Negative Linear Compressibility in $InH(BDC)_2$ from Framework Hinging. *J. Am. Chem. Soc.* **2017**, *139*, 15648−15651.

(10) Li, W.; Probert, M. R.; Kosa, M.; Bennett, T. D.; Thirumurugan, A.; Burwood, R. P.; Parinello, M.; Howard, J. A. K.; Cheetham, A. K. Negative Linear Compressibility of a Metal-Organic Framework. *J. Am. Chem. Soc.* **2012**, *134*, 11940−11943.

(11) Ogborn, J. M.; Collings, I. E.; Moggach, S. A.; Thompson, A. L.; Goodwin, A. L. Supramolecular Mechanics in a Metal−Organic Framework. *Chem. Sci.* **2012**, *3*, 3011−3017.

(12) Munn, R. W. Role of the Elastic Constants in Negative Thermal Expansion of Axial Solids. *J. Phys. C: Solid State Phys.* **1972**, *5*, 535.

(13) Fortes, A. D.; Suard, E.; Knight, K. S. Negative Linear Compressibility and Massive Anisotropic Thermal Expansion in Methanol Monohydrate. *Science* **2011**, *331*, 742−746.

(14) Shepherd, H. J.; Palamarciuc, T.; Rosa, P.; Guionneau, P.; Molnár, G.; Létard, J. F.; Bousseksou, A. Antagonism between Extreme Negative Linear Compression and Spin Crossover in $[Fe(Dpp)_2(NCS)_2]$·py. *Angew. Chem., Int. Ed.* **2012**, *51*, 3910−3914.

(15) Prawer, S.; Smith, T. F.; Finlayson, T. R. The Room Temperature Elastic Behaviour of CsH_2PO_4. *Aust. J. Phys.* **1985**, *38*, 63−83.

(16) Mariathasan, J. W. E.; Finger, L. W.; Hazen, R. M. High-Pressure Behavior of $LaNbO_4$. *Acta Cryst.* **1985**, *41*, 179−184.

(17) Goodwin, A. L.; Keen, D. A.; Tucker, M. G. Large Negative Linear Compressibility of $Ag_3[Co(CN)_6]$. *Proc. Natl. Acad. Sci. U. S. A.* **2008**, *105*, 18708−18713.

(18) Zeng, Q.; Wang, K.; Zou, B. Negative Linear Compressibility Response to Pressure in Multitype Wine-Rack Metal-Organic Frameworks. *ACS Mater. Lett.* **2020**, *2*, 291−295.

(19) Cai, W.; Gładysiak, A.; Anioła, M.; Smith, V. J.; Barbour, L. J.; Katrusiak, A. Giant Negative Area Compressibility Tunable in a Soft Porous Framework Material. *J. Am. Chem. Soc.* **2015**, *137*, 9296−9301.

(20) Jiang, X.; Luo, S.; Kang, L.; Gong, P.; Yao, W.; Huang, H.; Li, W.; Huang, R.; Wang, W.; Li, Y.; Li, X.; Wu, X.; Lu, P.; Li, L.; Chen, C.; Lin, Z. Isotropic Negative Area Compressibility over Large Pressure Range in Potassium Beryllium Fluoroborate and Its Potential Applications in Deep Ultraviolet Region. *Adv. Mater.* **2015**, *27*, 4851−4857.

(21) Seyidov, M. Y.; Suleymanov, R. A. Negative Thermal Expansion Due to Negative Area Compressibility in $TlGaSe_2$ Semiconductor with Layered Crystalline Structure. *J. Appl. Phys.* **2010**, *108*, No. 063540.

(22) Cliffe, M. J.; Goodwin, A. L. PASCal: A Principal Axis Strain Calculator for Thermal Expansion and Compressibility Determination. *J. Appl. Crystallogr.* **2012**, *45*, 1321−1329.

(23) Sheldrick, G. M. Crystal Structure Refinement with SHELXL. *Acta Crystallogr., Sect. C: Struct. Chem.* **2015**, *71*, 3−8.

(24) Sheldrick, G. M. A Short History of SHELX. *Acta Crystallogr., Sect. A: Found. Crystallogr.* **2008**, *A64*, 112−122.

(25) Dolomanov, O.; Bourhis, L. J.; Gildea, R. J.; Howard, J. A. K.; Puschmann, H. OLEX2: A Complete Structure Solution, Refinement and Analysis Program. *J. Appl. Crystallogr.* **2009**, *42*, 339−341.

(26) Brandenburg, K.; Putz, H. *Diamond: Crystal and Molecular Structure Visualization*; Crystal Impact: Bonn, Germany, 2008.

(27) Macrae, C. F.; Bruno, I. J.; Chisholm, J. A.; Edgington, P. R.; McCabe, P.; Pidcock, E.; Rodriguez-Monge, L.; Taylor, R.; van de Streek, J.; Wood, P. A. Mercury CSD 2.0 - New Features for the Visualization and Investigation of Crystal Structures. *J. Appl. Crystallogr.* **2008**, *41*, 466−470.

(28) Shen, G.; Wang, Y.; Dewaele, A.; Wu, C.; Fratanduono, D. E.; Eggert, J.; Klotz, S.; Dziubek, K. F.; Loubeyre, P.; Fatyanov, O. V.; Asimow, P. D.; Mashimo, T.; Wentzcovitch, R. M. M. Toward an

International Practical Pressure Scale: A Proposal for an IPPS Ruby Gauge (IPPS-Ruby2020). *High Pressure Res.* **2020**, *40*, 299−314.
(29) Datchi, F.; Dewaele, A.; Loubeyre, P.; Letoullec, R.; le Godec, Y.; Canny, B. Optical Pressure Sensors for High-Pressure−High-Temperature Studies in a Diamond Anvil Cell, *High Pressure Res.* 2007, *27* (4), 447−463, DOI: 10.1080/08957950701659593.
(30) Kurtz, S. K.; Perry, T. T. A Powder Technique for the Evaluation of Nonlinear Optical Materials. *J. Appl. Phys.* **1968**, *39*, 3798−3813.
(31) Rejnhardt, P.; Daszkiewicz, M. Crystal Structure, Theoretical and Vibrational Analysis of Isostructural Salts of l-Arginine Analogue, (*S*)-2-Amino-3-Guanidinopropanoic Acid. *J. Mol. Struct.* **2021**, *1229*, No. 129620.
(32) Devries, L. D.; Barron, P. M.; Hurley, E. P.; Hu, C.; Choe, W. "Nanoscale Lattice Fence" in a Metal-Organic Framework: Interplay between Hinged Topology and Highly Anisotropic Thermal Response. *J. Am. Chem. Soc.* **2011**, *133*, 14848−14851.
(33) Tchon, D.; Makal, A. Structure and Piezochromism of Pyrene-1-Carbaldehyde at High Pressure. *Acta Crystallogr., Sect. B: Struct. Sci. Cryst. Eng. Mater.* **2019**, *75*, 343−353.
(34) Kaźmierczak, M.; Patyk-Kaźmierczak, E.; Katrusiak, A. Compression and Thermal Expansion in Organic and Metal-Organic Crystals: The Pressure-Temperature Correspondence Rule. *Cryst. Growth Des.* **2021**, *21*, 2196.
(35) Ichikawa, M. Structure Isotope Effect in Hydrogen-Bonded Crystals-Similarity and Difference between Deuteration and Pressure Effect. *Pol. J. Chem.* **1998**, *72*, 230−240.
(36) Hodgson, S. A.; Adamson, J.; Hunt, S. J.; Cliffe, M. J.; Cairns, A. B.; Thompson, A. L.; Tucker, M. J.; Funnell, N. P.; Goodwin, A. L. Negative Area Compressibility in Silver(I) Tricyanomethanide. *Chem. Commun.* **2014**, *50*, 5264−5266.
(37) Jin, T.; Zhang, W. Geometric H/D Isotope Effect in a Series of Organic Salts Involving Short O−H···O Hydrogen Bonds between Carboxyl and Carboxylate Groups. *CrystEngComm* **2019**, *21*, 4238−4242.
(38) Ubbelohde, A. R.; Gallagher, K. J.; IUCr. Acid-Base Effects in Hydrogen Bonds in Crystals. *Acta Crystallogr.* **1955**, *8*, 71−83.
(39) Benedict, H.; Limbach, H. H.; Wehlan, M.; Fehlhammer, W. P.; Golubev, N. S.; Janoschek, R. Solid State ^{15}N NMR and Theoretical Studies of Primary and Secondary Geometric H/D Isotope Effects on Low-Barrier NHN−Hydrogen Bonds. *J. Am. Chem. Soc.* **1998**, *120*, 2939−2950.
(40) Shi, C.; Zhang, X.; Yu, C. H.; Yao, Y. F.; Zhang, W. Geometric Isotope Effect of Deuteration in a Hydrogen-Bonded Host−Guest Crystal. *Nat. Commun.* **2018**, *9*, 481.
(41) Katrusiak, A. Coupling of Displacive and Order-Disorder Transformations in Hydrogen-Bonded Ferroelectrics. *Phys. Rev. B* **1995**, *51*, 589.
(42) Cai, W.; Katrusiak, A. Giant Negative Linear Compression Positively Coupled to Massive Thermal Expansion in a Metal-Organic Framework. *Nat. Commun.* **2014**, *5*, 4337.
(43) Kalaiselvi, D.; Kumar, R. M.; Jayavel, R. Single Crystal Growth and Properties of Semiorganic Nonlinear Optical L-Arginine Hydrochloride Monohydrate Crystals. *Cryst. Res. Technol.* **2008**, *43*, 851−856.
(44) Nelmes, R. J.; Katrusiak, A. Evidence for Anomalous Pressure Dependence of the Spontaneous Strain in $PbTiO_3$. *J. Phys. C Solid State Phys.* **1986**, *19* (31), L725−L730.
(45) Zieliński, W.; Katrusiak, A. Colossal Monotonic Response to Hydrostatic Pressure in Molecular Crystal Induced by a Chemical Modification. *Cryst. Growth Des.* **2014**, *14* (9), 4247−4253.

https://doi.org/10.1021/acs.chemmater.3c00870
Chem. Mater. 2023, 35, 5160−5167